Functional redundancy of Rab27 proteins and the pathogenesis of Griscelli syndrome

Duarte C. Barral,[1] José S. Ramalho,[1] Ross Anders,[1] Alistair N. Hume,[1] Holly J. Knapton,[1] Tanya Tolmachova,[1] Lucy M. Collinson,[2] David Goulding,[2] Kalwant S. Authi,[3] and Miguel C. Seabra[1]

[1]Cell and Molecular Biology, Division of Biomedical Sciences, Faculty of Medicine, and
[2]Department of Biological Sciences, Faculty of Life Sciences, Imperial College, London, United Kingdom
[3]Centre for Cardiovascular Biology and Medicine, King's College London, London, United Kingdom

Griscelli syndrome (GS) patients and the corresponding mouse model *ashen* exhibit defects mainly in two types of lysosome-related organelles, melanosomes in melanocytes and lytic granules in CTLs. This disease is caused by loss-of-function mutations in *RAB27A*, which encodes 1 of the 60 known Rab GTPases, critical regulators of vesicular transport. Here we present evidence that Rab27a function can be compensated by a closely related protein, Rab27b. Rab27b is expressed in platelets and other tissues but not in melanocytes or CTLs. Morphological and functional tests in platelets derived from *ashen* mice are all within normal limits. Both Rab27a and Rab27b are found associated with the limiting membrane of platelet-dense granules and to a lesser degree with α-granules. Ubiquitous transgenic expression of Rab27a or Rab27b rescues *ashen* coat color, and melanocytes derived from transgenic mice exhibit widespread peripheral distribution of melanosomes instead of the perinuclear clumping observed in *ashen* melanocytes. Finally, transient expression in *ashen* melanocytes of Rab27a or Rab27b, but not other Rab's, restores peripheral distribution of melanosomes. Our data suggest that Rab27b is functionally redundant with Rab27a and that the pathogenesis of GS is determined by the relative expression of Rab27a and Rab27b in specialized cell types.

J. Clin. Invest. **110**:247–257 (2002). doi:10.1172/JCI200215058.

Introduction

Rab proteins are Ras-like monomeric GTPases that form a large family with 60 known genes identified in humans (1). Rab's have been implicated in the control of protein trafficking as regulators of several steps in vesicular transport such as vesicle budding, movement, and docking/fusion (2–5). Within this large family, there are Rab's that show unusually high identity and are considered isoforms, e.g., Rab1a and Rab1b. Rab isoforms are thought to be functionally related on the basis of structural homology. However, there is very little direct evidence to support this idea. In *Saccharomyces cerevisiae*, the Rab family (known as Ypt/Sec4) is composed of 11 members, with several close homologues clustering in subfamilies, i.e., Ypt31 and 32, and Ypt51, 52, and 53 (6, 7). Ypt31p and Ypt32p play a role in the budding of vesicles from the *trans*-Golgi apparatus (8). Cells can tolerate the disruption of one of the two genes but not the simultaneous deletion of both, suggesting that they perform overlapping functions (8, 9). Ypt51p (also called Vps21), Ypt52p, and Ypt53p are involved in early steps of the endocytic pathway and in the sorting of vacuolar hydrolases (10, 11). In this subfamily, Ypt51 seems to predominate functionally because Ypt51 deletion mutants present a severe phenotype that is aggravated in double or triple mutants (10).

In mammals, Rab27a and its isoform Rab27b, which exhibits 71% identity at amino acid level, form one such Rab subfamily. In humans, mutations in *RAB27A* cause Griscelli syndrome (GS), an autosomal recessive disorder characterized by pigment dilution of the hair and an uncontrolled T lymphocyte and macrophage activation syndrome known as hemophagocytic syndrome (12, 13). At the cellular level, this disease reflects dysfunction of at least two types of specialized lysosome-related organelles: melanosomes in melanocytes and lytic granules in CTLs (5, 14). GS melanocytes show an accumulation of mature melanosomes in the perinuclear region rather than even dispersion observed in wild-type cells, consistent with a defect in melanosome transport (15). GS CTLs exhibit a reduced cytotoxic activity due to defective lytic granule release (13). The corresponding mouse model for GS, *ashen* (*Rab27a*^{ash}), exhibit a loss-of-function mutation in *Rab27a* (16). Strikingly, melanosomes are clustered in the perinuclear region of melanocytes (16–18),

Received for publication January16, 2002, and accepted in revised form June 6, 2002.

Address correspondence to: Miguel C. Seabra, Cell and Molecular Biology Section, Faculty of Medicine, Imperial College, Sir Alexander Fleming Building, Exhibition Road, London SW7 2AZ, United Kingdom. Phone: 44-207-594-3024; Fax: 44-27-594-30-15; E-mail: m.seabra@ic.ac.uk.

Conflict of interest: No conflict of interest has been declared

Nonstandard abbreviations used: Griscelli syndrome (GS); Hermansky-Pudlak syndrome (HPS); Rab geranylgeranyl transferase (RGGT); storage pool deficiency (SPD); platelet-rich plasma (PRP); PBS with 0.2% Tween-20 (PBS_T); electron microscopy (EM); postnuclear supernatant (PNS); cytomegalovirus (CMV).

and *ashen* CTLs are unable to kill targets due to impaired granule exocytosis (19, 20).

A few other human genetic diseases reflect defects in lysosome-related organelle biology. One of those is Hermansky-Pudlak syndrome (HPS), an autosomal recessive disorder characterized by oculocutaneous albinism and hemorrhagic episodes due to platelet storage pool deficiency (SPD) (21). Mouse models of this disease are characterized by pigment dilution and prolonged bleeding times. Fifteen nonallelic mouse mutants have been proposed to be HPS models, and three gene mutations have been described to date in humans, suggesting that this disorder is genetically heterogeneous (14, 22). One of the HPS mouse models is the *gunmetal* mouse (*Rggta*^{gm}). The bleeding disorder in these mice involves macrothrombocytopenia, a reduction in platelet dense and α-granule contents, and morphological defects in megakaryocytes that affect platelet maturation (23, 24). These mice possess a mutation in the α-subunit of Rab geranylgeranyl transferase (RGGT), a heterodimeric enzyme that catalyses the covalent attachment of two geranylgeranyl isoprenoids to the C terminus of Rab proteins (25–27). This mutation results in an 80% reduction in the activity of this enzyme (26). Interestingly, the reduced level of RGGT activity in *gunmetal* mice affects only a selected number of tissues, hence the HPS-like phenotype. Melanocytes and megakaryocytes/platelets are the most affected. In platelets, a few Rab's are affected by the hypoactivity of the enzyme, including Rab27a (26).

The availability of naturally occurring Rab27a (*ashen*) mouse mutants provided an opportunity to address the issue of Rab functional redundancy in mammalian cells. Here we show that *ashen* mice exhibit normal platelet morphology and function, suggesting that Rab27b compensates for the loss of Rab27a in these cells. Furthermore, transgenic expression of Rab27b rescues *ashen* phenotype. Our results suggest that Rab27b is functionally redundant with Rab27a and provide clues to the pathogenesis of GS.

Methods

Mice. *Ashen* mice (C3H/HeSn-*ash*/*ash*) were purchased from The Jackson Laboratory (Bar Harbor, Maine, USA). The *gunmetal* mice (C57BL/6J-*gm*/*gm*) were kindly supplied by Richard Swank (Roswell Park Cancer Institute, Buffalo, New York, USA). C57BL/6 and C3H/He wild-type mice were purchased from B&K Universal Ltd. (Hull, East Yorkshire, United Kingdom). All mice were bred and maintained under United Kingdom project license PPL 70/5071 at the Central Biomedical Services of Imperial College, London, United Kingdom.

Tissue and cell lysis and platelet purification. C57BL/6 mice were perfused by cardiac injection of PBS. Tissues were collected and homogenized thoroughly in 3 vol of lysis buffer (50 mM sodium HEPES, pH 7.2, 10 mM NaCl, 1 mM dithiothreitol, 0.5 mM PMSF, 5 μg/ml pepstatin, 5 μg/ml aprotinin, and 5 μg/ml leupeptin). The homogenate was centrifuged at 7,000 *g* at 4°C for 10 minutes to sediment unbroken cells and cell nuclei. The postnuclear supernatant (PNS) was then centrifuged at 100,000 *g* for 1 hour at 4°C to pellet membrane fractions. To obtain platelet lysates, blood was drawn by cardiac puncture under terminal anesthesia in 1:10 sodium citrate, spun at 120 *g* for 20 minutes at room temperature, and the upper phase (platelet-rich plasma [PRP]) was saved. After adding 22 μl of 0.3 M citric acid per milliliter of PRP, the PRP was spun at 1,200 *g* for 15 minutes at room temperature, and the supernatant discarded. The pellet was resuspended in washing buffer (134 mM NaCl, 12 mM $NaHCO_3$, 2.9 mM KCl, 0.34 mM Na_2HPO_4, 1 mM $MgCl_2$, 10 mM sodium HEPES, 5 mM glucose, 3 g/l BSA, 10% citrate-citric acid-dextrose, pH 7.4), and centrifuged as done previously. The pellet was homogenized in lysis buffer and mechanically disrupted by serial passages through a 21-gauge needle. Melan-a and CTL cell pellets were homogenized in the same way as platelets and centrifuged at 100 *g* for 10 minutes at 4°C to obtain the PNS. The protein concentration of all lysates and fractions was determined using Coomassie Plus Protein Assay Reagent (Perbio Science UK Ltd., Tattenhall, Cheshire, United Kingdom).

Immunoblotting. Protein extracts were subjected to SDS-PAGE on 12.5% acrylamide gels and then transferred to a PVDF membrane using a Hoeffer transfer apparatus (90 minutes at 500 mA). The membranes were allowed to dry and then were blocked with 5% skimmed milk in PBS with 0.2% Tween-20 (PBS_T) for 1 hour at room temperature. The membranes were then incubated with primary Ab diluted in PBS_T. After washing, blots were incubated with secondary Ab, peroxidase-labeled, diluted in blocking buffer, and developed using the Supersignal West Pico Chemiluminescent Substrate (Pierce Chemical Co.) according to the manufacturer's directions. Anti-Rab27a mouse mAb 4B12 (17), affinity-purified anti-Rab27b rabbit polyclonal Ab S086 (see below), anti-calnexin rabbit polyclonal Ab (1:5,000; StressGen Biotechnologies Corp., Victoria, British Columbia, Canada), and anti–c-myc mouse mAb (1:400; Calbiochem-Novabiochem Corp., Beeston, Nottingham, United Kingdom) were used for immunoblots. The secondary Ab's used were horseradish peroxidase-labeled sheep anti-mouse (1:10,000; Amersham Pharmacia Biotech, Little Chalfont, Buckinghamshire, United Kingdom) and goat anti-rabbit (1:10,000; DAKO Ltd., Ely, Suffolk, United Kingdom).

Ab affinity-purification. S086 and N688 immune serum were applied to 1 ml of an affinity column prepared by cross-linking 2 mg of bacterially expressed Rab27a or Rab27b (17) to AminoLink Coupling Gel (Pierce Chemical Co.) as directed by the manufacturer. The column was washed with 20 ml of 10 mM Tris-HCl (pH 7.5), followed by 20 ml of 10 mM Tris-HCl (pH 7.5) containing 0.5 M NaCl. Bound IgG was

eluted with 0.1 M glycine (pH 2.9) and collected in 1-ml fractions containing 0.1 ml of 1 M Tris-HCl (pH 8.0).

Bleeding time assays. Mice aged 9–12 weeks were locally anesthetized. One to three millimeters of the distal mouse tail was removed, and the remaining tail was immediately immersed in isotonic saline (0.9% NaCl) at 37°C. The time required for a complete cessation of the blood stream was defined as the bleeding time. Bleeding time measurements exceeding 10 minutes were interrupted at that time by cauterization of the tail.

Platelet counts. Blood samples from mice aged 9–11 weeks were drawn as described above and centrifuged at 180 *g* for 15 minutes at room temperature to separate the PRP. Platelets were diluted 1:2,000, and 50 μl were counted in a Beckman Coulter Counter (model ZM; Beckman Coulter UK Ltd., High Wycombe, Buckinghamshire, United Kingdom) set to count all particles between 0.6 and 27 μm^3.

Determination of platelet size. Whole blood (50 μl) of mice aged 9–14 weeks, drawn as described above, was stained with 10 μg/ml of FITC-labeled anti-mouse CD41 (Integrin α_{IIb} chain; BD PharMingen, Cowley, Oxfordshire, United Kingdom) diluted in isotonic saline. After an incubation of 30 minutes, 2 μl of stained whole blood was diluted in 1 ml of PBS with 0.1% sodium azide (1:500) and analyzed in a FACSCalibur (Becton Dickinson Immunocytochemistry Systems, Cowley, Oxfordshire, United Kingdom) using CELLQuest version 3.1f software.

Determination of endogenous vWF levels. Platelets were isolated, homogenized, and total protein quantified as described above. ELISA plates were coated overnight at room temperature with 100 μl of anti-vWF (DAKO Ltd.) diluted (1:600) in PBS and blocked for 1 hour at room temperature with 300 μl of blocking buffer (PBS with 0.1% Tween 20, 0.2% gelatin, and 1 mM EDTA). Samples (100 μl per well) diluted in PBS with 0.5% Triton X-100, 0.1% gelatin, and 0.5 mM EDTA were incubated for 1 hour at room temperature, and the plates were washed twice with blocking buffer. The plates were then incubated for 1 hour with horseradish peroxidase–labeled anti-vWF (1:500) in blocking buffer. After washing the plates three times with blocking buffer and twice with PBS, the reactions were developed with 100 μl 2-2′-azino-bis(3-ethylbenzthiazoline-6-sulfonic acid) (Sigma-Aldrich, Gillingham, United Kingdom) and stopped with same volume of 1% SDS.

Aggregations and 5-hydroxytryptamine release assays. The aggregations were performed according to methods described previously (28). Blood from mice aged 10–16 weeks was drawn as described above, centrifuged at 130 *g* for 20 minutes at room temperature, and PRP was isolated. PRP was then incubated with 0.1 μCi/ml of 5-hydroxy-3-indolyl([1-^{14}C]ethyl-2-amine)creatinine sulphate (^{14}C-5-HT) (Amersham Pharmacia Biotech) for 1 hour at 37°C. After adding 22 μl of 0.3 M citric acid per milliliter of PRP, PRP was centrifuged at 1,200 *g* for 15 minutes at room temperature. The supernatant was discarded and the pellet washed with Tyrode's buffer (138 mM NaCl, 2.9 mM KCl, 12 mM $NaHCO_3$, 0.36 mM $NaPO_4$, 5.5 mM glucose, 10 mM HEPES, 0.4 mM $MgCl_2$, pH 7.4) and resuspended in the same buffer. For each aggregation, 150 μl of washed platelets was used. After incubating the platelets at 37°C for at least 3 minutes, different doses of thrombin or collagen were added to the stirring samples, and the aggregation traces were recorded in an aggregometer (model 600B; Payton Scientific Inc., Buffalo, New York, USA). After 5 minutes, the reaction was stopped with 50 μl of ice-cold 16 mM EDTA with 1% paraformaldehyde (pH 7.4). The reactions were placed on ice until a centrifugation step (9,500 *g* for 5 minutes at 4°C). The number of counts in 100 μl of supernatant, representing released 5-hydroxytryptamine (5-HT), was determined in a β-counter (Packard liquid scintillation analyser model 1900TR; Perkin Elmer Life Sciences, Boston, Massachusetts, USA) with 4 ml of scintillation fluid and expressed as percentage of release of the total 5-HT present in platelets.

Determination of endogenous 5-HT levels. Endogenous 5-HT was measured as described previously (29). Essentially, 4 vol of ice-cold EDTA 0.4% in saline was added to PRP. After spinning at 14,700 *g* for 2 minutes, the platelets were lysed in 250 μl of double-distilled water. After precipitating the proteins in each sample with 50 μl of 6 M trichloroacetic acid, the supernatant was saved and added to 1 ml of *O*-phtaldialdehyde. After heating at 100°C for 10 minutes, the samples were cooled on ice and washed with chloroform. Finally, the fluorescence was read in a luminescence spectrometer (model LS50B; Perkin Elmer Instruments, Beaconsfield, Buckinghamshire, United Kingdom) with activation and emission wavelengths at 360 and 475 nm, respectively, using FL WinLab version 3.0 software. A standard curve was generated with different concentrations of 5-HT (Sigma-Aldrich) ranging from 1.5 to 100 ng/ml.

Detection of P-selectin at the platelet surface. Whole blood from mice aged 14–21 weeks was drawn as described above and diluted 1:6 in Tyrode's buffer within 15 minutes. Biotinylated anti–P-selectin Ab (5 μg/ml; BD PharMingen), diluted in saline and different concentrations of PMA (Calbiochem-Novabiochem Corp.), diluted in PBS with 1% BSA were incubated with 50 μl of diluted blood for 1 hour at room temperature. Anti–CD41 FITC (gpIIb; BD PharMingen) Ab and streptavidin PE (both at 10 μg/ml) were incubated at room temperature for the same time, and samples were fixed with 1 vol of Tyrode's buffer with 1% paraformaldehyde (pH 7.4) for 30 minutes at room temperature. Finally, the samples were diluted 1:20 in Tyrode's buffer and kept for up to 24 hours at 4°C before analysis. The analysis was performed in a FACSCalibur (Becton Dickinson Immunocytochemistry Systems) using CELLQuest version 3.1f software.

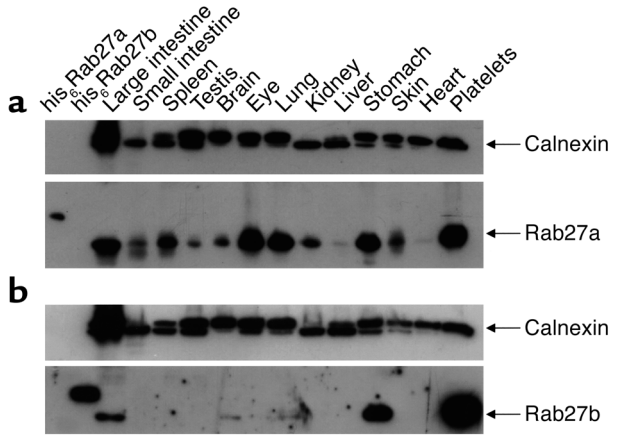

Figure 1
Tissue distribution of Rab27a and Rab27b. Tissues from perfused mice were lysed, the postnuclear supernatant was ultracentrifuged, and identical amounts of protein (35 μg) from the pellet fractions were subjected to SDS-PAGE and immunoblot analysis as described in Methods. Monoclonal anti-Rab27a Ab 4B12 was used to probe Rab27a (**a**) and affinity-purified polyclonal anti-Rab27b Ab S086 to probe Rab27b (**b**). Anti-calnexin Ab recognizing a ubiquitous endoplasmic reticulum-membrane protein (ER-membrane protein) was used as a loading control. Recombinant his_6Rab27a and his_6Rab27b (25 ng) were used as controls for Ab specificity.

Electron microscopy and immunoelectron microscopy. For the evaluation of the quantity of dense granules, platelets in PRP were pelleted gently and fixed in 2% paraformaldehyde/1.5% glutaraldehyde. The pellets were osmicated, stained with tannic acid, and embedded in Epon for ultrathin-section electron microscopy (EM). The number of dense granules per platelet was estimated using stereological methods. The average volume of platelets was taken to be 3.3 fl (30). The average volume of dense granules was estimated by measuring the diameter of granules in thin sections. The largest granules present were measured in an attempt to represent the true diameter. The average volume of dense granules in both heterozygous and homozygous *ashen* platelets was determined to be 0.008 fl. Ultrathin sections were cut from Epon-embedded pellets and chosen randomly for stereology. Micrographs were taken randomly over the chosen sections at ×13,000 magnification. A double-lattice grid (D64) was used to gather data (30). Points on the grid touching the cytoplasm and points touching dense granules were counted on 20 negatives for each cell type (200 platelets each). Using these data, the volume of dense granules per volume of cytoplasm was calculated, and hence the number of dense granules per platelet. For immuno-EM, platelets were fixed in 4% paraformaldehyde/0.1% glutaraldehyde in PBS for 1 hour on ice, washed three times with PBS for 15 minutes, and infiltrated with 2.3 M sucrose in PBS overnight at 4°C. They were then frozen onto the microtome stub in liquid nitrogen and sectioned on an ultracryomicrotome (Leica Ultracut; Leica Microsystems [UK] Ltd., Milton Keynes, Buckinghamshire, United Kingdom) at 60 nm. The sections were blocked with 0.02 M glycine in PBS for 10 minutes. Sections were further blocked with 10% FCS in PBS for 30 minutes. Affinity-purified anti-Rab27a polyclonal Ab N688 and anti-Rab27b S086 were incubated for 30 minutes, and after washing, the sections were incubated with 10 nm protein A–gold and washed again. Sections were fixed in 2.5% glutaraldehyde in PBS for 5 minutes, washed with PBS and then with double-distilled water. After contrasting with 3% uranyl acetate in methylcellulose on ice for 10 minutes, the grids were air-dried and analyzed.

Generation of transgenic mice and genetic crosses. A fragment containing the human cDNA for Rab27a or Rab27b fused to a myc-epitope was generated by PCR and subcloned into the *Xho*I site of the eukaryotic expression vector pCAGGS, downstream of the chicken β-actin promoter (31–34). Myc-tagged Rab27a/b is thus downstream of the ubiquitous chicken β-actin promoter and cytomegalovirus immediate-early (CMV-IE) enhancer, upstream of the rabbit β-globin poly(A) signal. For each construct, a 3.4-kb *Spe*I-*Bam*HI fragment was isolated and microinjected into the pronuclei of one-cell stage embryos from a C57BL/6JxCBA background collected from superovulated female mice (35, 36). Microinjected eggs were transferred at the two-cell stage into the oviducts of pseudopregnant recipient females. Mice born were routinely screened for incorporation of the transgene by PCR with primers JR135 (5′-GACAGAATGTGGAGAAAGCTGTAGAAACCC) and JR148 (5′-CTTTATTAGCCAGAAGTCAGATGCTCAAGG). Positive mice were crossed with *ashen* (*ash*/*ash*) mice on a C57BL/6J background obtained by repeated backcrossing (over five generations) with wild-type C57BL/6J mice to generate heterozygous *ashen* (+/*ash*) mice carrying the transgene. These were then crossed again as above to generate homozygous *ashen* (*ash*/*ash*) mice carrying the transgene. These mice were evaluated visually for the rescue of the coat color. The *ashen* mutation was

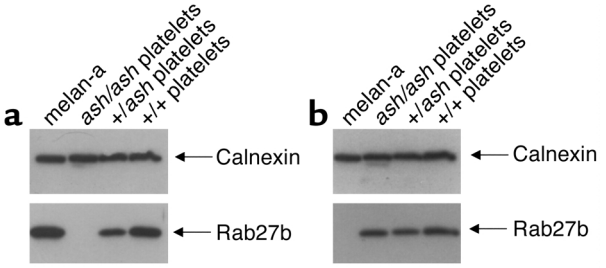

Figure 2
Expression of Rab27a and Rab27b in melanocytes and platelets. Platelets from wild-type (C3H/$He^{+/+}$), homozygous (*ash*/*ash*), and heterozygous (+/*ash*) *ashen* mice and a melanocytic cell line (melan-a) were lysed, and identical amounts of protein (13 μg) from total lysates (for platelets) or postnuclear supernatants (for melan-a cells) were subjected to SDS-PAGE and immunoblotting as described in Methods. Monoclonal anti-Rab27a Ab, 4B12 was used to probe Rab27a (**a**) and affinity-purified polyclonal anti-Rab27b Ab S086 to probe Rab27b (**b**). Anti-calnexin Ab recognizing a ubiquitous ER-membrane protein was used as a loading control.

Table 1
Bleeding times, number of platelets, and platelet size in *ashen*, *gunmetal,* and respective controls

Strain	Bleeding times (min)	Number of platelets ($\times 10^8$)/ml	Platelet size (arbitrary units)
C3H/He$^{+/+}$	5.51 ± 3.28	1.59 ± 0.73	252.97 ± 17.23
+/ash	4.61 ± 3.31	1.67 ± 0.48	229.18 ± 20.53
ash/ash	5.02 ± 3.68	1.68 ± 0.43	247.5 ± 15.97
C57BL/6$^{+/+}$	4.29 ± 2.77	1.47 ± 0.5	220.64 ± 12.2
+/gm	3.83 ± 1.91	1.34 ± 0.31	234.19 ± 12.07
gm/gm	>10**	0.52 ± 0.13**	463.45 ± 21.02**

Values are the mean ± SD. Six mice were used in each case. For the number of platelets three counts were made and the number of particles in buffer discounted. The statistical analysis was performed using a Kruskal-Wallis nonparametric test for bleeding times, a linear regression with clusters test for number of platelets, and finally an ANOVA for platelet size. $^{**}P < 0.001$.

screened by PCR with primers ASH1 (5′-ACCTGACAAATGAGCAAAGTTTCCTCAATG) and ASH2 (5′-GGAGCAGGGCAGGGCTGGGGAAACCACTCG) followed by restriction enzyme analysis with *Taq*I and *Rsa*I.

Melanocyte cell culture and transfection. The derivation of primary melanocytes was described previously (37). Briefly, skins from neonatal *ashen* mice (1–3 days old) were incubated with 5 ml of bovine trypsin (5 mg/ml in PBSA) for 1 hour at 37°C. The epidermis was then peeled from the dermis using sterile forceps and cut into smaller fragments using a scalpel blade. These fragments were then placed in 2 ml of melanocyte medium, RPMI-1640, supplemented with 10% FCS, 100 U/ml penicillin G, 100 U/ml streptomycin, 200 nM PMA, and 200 pM cholera toxin (Calbiochem-Novabiochem Corp.) supplemented with 5 μg/ml soybean trypsin inhibitor per skin. This mixture was then aspirated through the nozzle of a 5-ml combitip and the resulting cell suspension was plated onto mitomycin C–treated Xb2 murine keratinocyte–derived feeder cells. Primary cultures of murine melanocytes were maintained in melanocyte medium at 37°C with 10% CO_2. Melan-ash cells were a gift from John A. Hammer III (National Heart, Lung, and Blood Institute, National Institutes of Health, Bethesda, Maryland, USA) (18) and were cultured in melanocyte medium without cholera toxin. Cells were transiently transfected using Lipofectamine 2000 (Invitrogen Corp., San Diego, California, USA) and plasmid DNAs purified with a QIAGEN mini prep kit (QIAGEN Inc., Crawley, West Sussex, United Kingdom). Plasmids pEGFP-Rab1a (17), pEGFP-Rab27a (31), and pEGFP-Rab27b (31) were described elsewhere, and pEGFP-Rab3a was made by digesting pBTM116-Rab3a (38) with *Eco*RI and *Bam*HI and subcloning into *Eco*RI/*Bam*HI–digested pEGFP-C2. DNAs (1 μg) were diluted in 50 μl of OPTI-MEM I medium (Invitrogen Corp.) and added to 50 μl of the same medium containing 2.5 μl of Lipofectamine 2000 reagent. After incubating for 30 minutes at room temperature, this mixture was diluted 1:2 in OPTI-MEM I and added to cells grown on coverslips. After 6 hours, the OPTI-MEM I medium was removed, and complete medium was added. Twenty-four to 32 hours after transfection, cells were permeabilized for 5 minutes at room temperature in permeabilization buffer (80 mM PIPES, pH 6.8, 5 mM EGTA, 1 mM $MgCl_2$, and 0.05% saponin) and immediately fixed in 3% paraformaldehyde in PBS for 15 minutes. Cells were washed three times with PBS, and the fixative was quenched with 50 mM NH_4Cl. Coverslips were mounted in Immuno-Fluor medium (ICN Biomedicals, Thame, Oxfordshire, United Kingdom) and observed with a Leica DM-IRBE confocal microscope. Images were processed using Leica TCS-NT software and Adobe Photoshop 5.5 software (Adobe Systems Inc., Mountain View, California, USA). All images presented are single sections in the *z* plane.

Results

Rab27b is expressed in platelets but not in melanocytes or CTLs. We first compared the distribution of Rab27a and Rab27b in mouse tissues by immunoblotting. We used affinity-purified specific, non–cross-reacting Ab's to probe for Rab27a (monoclonal 4B12) and Rab27b (polyclonal affinity-purified S086). As displayed in Figure 1a, Rab27a shows a broad distribution among the tissues tested. We detected high expression in large intestine, spleen, eye, lung, stomach, and platelets. This is in general agreement with previous data regarding both protein levels in rat tissues (39) and mRNA levels in human and mouse tissues (31, 40). The major site of Rab27b expression appears to be in platelets and to a lesser extent, the gastrointestinal tract (Figure 1b). We detected little, if any, expression in other tissues.

We next determined which Rab27 isoforms are expressed in the cell types implicated in GS and HPS. As expected, Rab27a was detected in a melanocytic cell

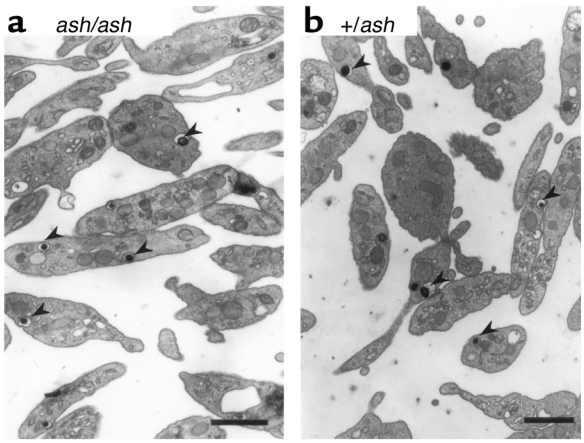

Figure 3
EM of *ashen* platelets. Platelets were isolated, fixed, and processed for EM as described under Methods. *Ashen* (*ash/ash*) platelets (**a**) appear normal when compared with heterozygous (*+/ash*) controls (**b**). Typical dense granules (arrowheads) are shown. The granules are electron dense due to their high calcium content. Bars, 1 μm.

Table 2
Amount of platelet endogenous serotonin (5-HT) in *ashen, gunmetal,* and respective controls

Strain	5-HT (μg/10^9 platelets)
C3H/He$^{+/+}$	1.59 ± 0.35
ash/ash	1.25 ± 0.22
C57BL/6$^{+/+}$	1.67 ± 0.48
gm/gm	0.8 ± 0.26*

Values are the mean ± SD. Twelve C3H/He$^{+/+}$ and *ash/ash* mice were tested in pools of two mice and ten C57BL/6$^{+/+}$, and *gm/gm* mice were tested in the same way. The statistical analysis was performed using an ANOVA test. *$P < 0.01$.

line originated from a C57BL/6 mouse, melan-a (17, 41), and in heterozygous *ashen* (+/*ash*) and wild-type (C3H/He$^{+/+}$) platelets (Figure 2a). However, no protein could be detected in homozygous *ashen* (*ash/ash*) mutants, presumably because the truncated mutant protein is unstable (Figure 2a). Strikingly, no signal could be detected for Rab27b in melan-a cells, even after prolonged exposure of the film (Figure 2b). In CTLs, we have reported similar results previously, i.e., no detectable expression of Rab27b (19). Also, Rab27b expression is not affected in *ashen* mice since homozygous (*ash/ash*) mice express normal levels of this protein (Figure 2b). These observations raise the possibility of functional compensation between both isoforms in platelets, but not in melanocytes or CTLs due to absent expression.

Ashen mice show normal platelet morphology and function. We then decided to analyze in detail the platelet phenotype of *ashen* mice. We started by measuring the bleeding times after injury in *ashen* (*ash/ash*) mutants and in heterozygous (+/*ash*) and wild-type (C3H/He$^{+/+}$) controls. As summarized in Table 1, the average bleeding time for the three strains is not significantly different. We also performed platelet counts by measuring the number of particles in PRP (Table 1) and found no significant difference between *ashen* and respective controls (heterozygous and wild-type mice). We next investigated platelet size by flow cytometry using an anti-CD41 (gpIIb) Ab. The arithmetic means of forward light scatter distributions, which reflect particle size, are shown in Table 1 and indicate that *ashen* platelets are not significantly different from controls. In all three experiments, we used *gunmetal* platelets as positive controls. We were able to confirm that *gunmetal* mice exhibit thrombocytopenia with increased bleeding times and platelet size.

SPD, as seen in HPS mouse models, including *gunmetal*, is defined by severe reduction of identifiable dense granules when observed by EM. We used EM to count the number of dense granules per platelet in *ashen* (Figure 3a) and in heterozygous controls (Figure 3b) and found no significant differences (5.97 ± 3.78 granules in *ashen* versus 6.18 ± 3.54 granules for controls) in a total of 200 platelets, indicating that these mice do not have a storage pool deficiency. To confirm these findings, we analyzed the amount of endogenous serotonin, or 5-HT, which is stored in platelet-dense granules and concluded that *ashen* platelets have normal levels of endogenous 5-HT (Table 2). *Gunmetal* mice (*gm/gm*), which present a mild SPD, showed about half of the normal endogenous 5-HT levels (Table 2), confirming previous findings (23).

The levels of α-granule components were also investigated. For this, the amount of endogenous vWF was assayed by sandwich ELISA. As shown in Figure 4a, *ashen* show normal levels of endogenous vWF, since the curves for homozygous (*ash/ash*) mice and heterozygous (+/*ash*) controls coincide. We also tested *gunmetal* mice (Figure 4b), which show approximately half of the endogenous vWF levels observed in heterozygous (+/*gm*) controls.

Finally, we evaluated the functional capacity of *ashen* platelets. We analyzed the release of dense and α-granule components and monitored platelet aggregation. *Ashen* platelets aggregate normally when stimulated with 2 U/ml of thrombin (Figure 5a). The percentage of aggregation after 5 minutes was not significantly different in several independent experiments (48.6% ± 10.4% for wild-type versus 36.3% ± 9.2% for *ashen*). We obtained similar results for lower doses of thrombin (0.5 and 1 U/ml) and collagen (10 μg/ml) (data not shown). In the same experiment, the release of ^{14}C-5-HT to the medium upon activation was determined and found to be within normal limits (77.5% ± 3.7% for *ashen* versus 76.75% ± 2.85% for wild-type). Similar results were obtained when platelets were stimulated with 10 μg/ml of collagen (data not shown). These results indicate that *ashen* platelets aggregate and release their dense granule contents normally when stimulated with thrombin or collagen.

The α-granule release capacity was investigated by flow cytometry through the detection of P-selectin (a mainly α-granule membrane component) at the platelet surface upon activation with PMA. We observed no significant difference between *ashen*

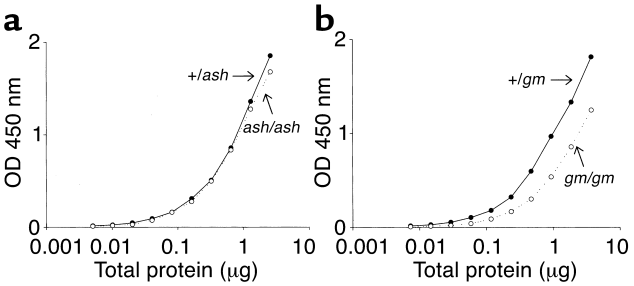

Figure 4
ELISA detection of endogenous vWF. Platelets from *ashen* homozygous (*ash/ash*) and heterozygous mice controls (+/*ash*) (**a**) and from *gunmetal* homozygous (*gm/gm*) and heterozygous mice controls (+/*gm*) (**b**) were lysed and the indicated amount of total protein incubated with 100 μl of buffer in a sandwich ELISA (see Methods). Each step corresponds to a 1:2 dilution, and duplicates were made for each point. The results are representative of three independent experiments. The OD_{450nm} value from the blank reaction (buffer only) was subtracted.

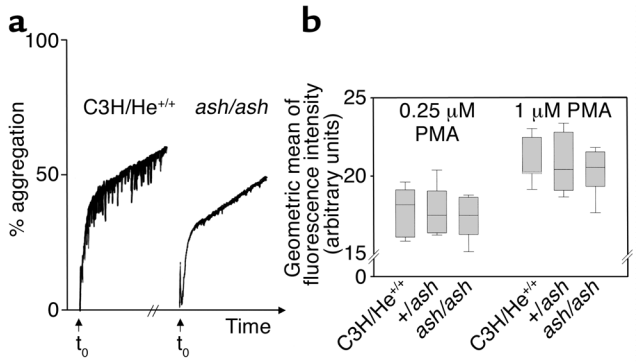

Figure 5

Platelet aggregation and expression of P-selectin at cell surface upon activation. (**a**) The aggregation capacity of homozygous *ashen* mice (*ash/ash*) and wild-type C3H/He mice (C3H/He$^{+/+}$) was tested, measuring the increasing light transmission through a platelet suspension. The agonist (thrombin at 2 U/ml) was added at t_0, and the traces were recorded for 5 minutes. The experiment was repeated independently, and the results were not significantly different (see text). The 0% corresponds to the light transmission of the resting platelet suspension and the 100% to the transmission of light in suspension buffer (or totally aggregated platelets). (**b**) The expression of P-selectin (mainly localized in α-granule membrane) at the surface of platelets upon stimulation with PMA was used to test α-granule release capacity. Platelets in whole blood were identified with an anti–CD41 (gpIIb) Ab. The geometric mean of the population of platelets labeled with anti–P-selectin Ab was plotted. Triplicates were done for each mouse, and six mice were tested in each case. Boxes represent the 25th and 75th percentiles, and median is represented by horizontal line inside the boxes. The error bars represent the 5th and 95th percentiles. The statistical analysis was performed using an ANOVA test, and the were results found not to be significantly different. The negative controls (without anti–P-selectin Ab) showed less that 2% activated platelets.

mutants and respective controls for PMA-induced P-selectin expression at two different doses of the phorbol ester (Figure 5b).

Rab27a and b colocalize in platelet granules. We then sought to localize both Rab27a and Rab27b proteins within platelets. Using non–cross-reacting, affinity-purified Ab's (anti-Rab27a N688 and anti-Rab27b S086), we detected both proteins associated with the limiting membrane of dense granules by immuno-EM (Figure 6). While most of the labeling was found in dense granules, some degree of labeling on α-granule membranes was evident, especially in the case of Rab27a. No labeling was obtained in control experiments where primary Ab's were abolished (data not shown).

Transgenic expression of Rab27b rescues ashen coat color phenotype. Our data suggested thus that Rab27b compensates for the loss of Rab27a in *ashen* platelets, but not melanocytes or CTLs, because of absent expression. To test this hypothesis directly, we produced transgenic mouse lines expressing myc-tagged Rab27b under the control of the strong chicken β-actin ubiquitous promoter as well as similar control lines expressing Rab27a (Figure 7a). These mice were crossed twice with *ashen* homozygous mice to obtain transgenic homozygous *ashen* mice. The progeny was genotyped (Figures 7, b and c) and examined for coat color (Figure 7, d and e). The mice that were homozygous *ashen* and carried the Rab27b transgenic insertion (*ash/ash,* –/tg^{Rab27b}) exhibited dark coat color, very similar to wild-type controls, whereas homozygous *ashen* mice without the transgene were light grey (*ashen*-like). In some cases, transgenic mice presented spots or small areas of lighter grey, which could be due to variegation. The control Rab27a transgenic lines (*ash/ash,* –/tg^{Rab27a}) also rescued the coat color phenotype of homozygous *ashen* mice, as expected (Figure 7e). We also analyzed the levels of expression of transgenic proteins in tissues from the rescued mice by immunoblot analysis. We found that expression levels varied considerably from tissue to tissue as well as from line to line. Nevertheless, the maximum levels of expression of transgenes did not exceed two- to three-fold the levels of the highest-expressing levels of endogenous proteins. Furthermore, the highest expression levels were comparable between Rab27a and Rab27b transgenic mice (data not shown).

We then analyzed melanocytes derived from the rescued transgenic lines. We produced primary cultures from skin melanocytes and observed the distribution of the melanosomes within them. The cultures were mixed populations of melanocytes showing widespread distribution of melanosomes throughout the entire cell volume and melanocytes showing clumping of melanosomes in the perinuclear region as observed in *ashen* melanocytes (Figure 8). The percentage of melanocytes exhibiting complete widespread distribution of melanocytes was 58.4% ± 5.6% (n = 178) for *ash/ash,* –/tg^{Rab27a} (Figure 8a), 39.8% ± 0.2% (n = 171) for *ash/ash,* –/tg^{Rab27b} (Figure 8b) and 9.5% ± 2.1% (n = 190) for *ash/ash* (Figure 8c). The numbers obtained for transgenic melanocytes are likely to be an underestimate

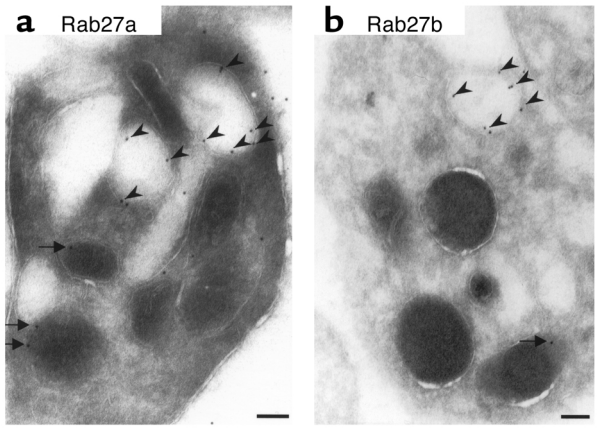

Figure 6

Immuno-EM of wild-type platelets. Platelets from C3H/He$^{+/+}$ mice were processed for immuno-EM as described in Methods. Affinity-purified polyclonal anti-Rab27a Ab N688 was used to probe for Rab27a (**a**) and affinity-purified polyclonal anti-Rab27b S086 to probe for Rab27b (**b**). The labeling was found mainly in dense granules (arrowheads). Some labeling was also detected in α-granules (arrows). Bars, 100 nm.

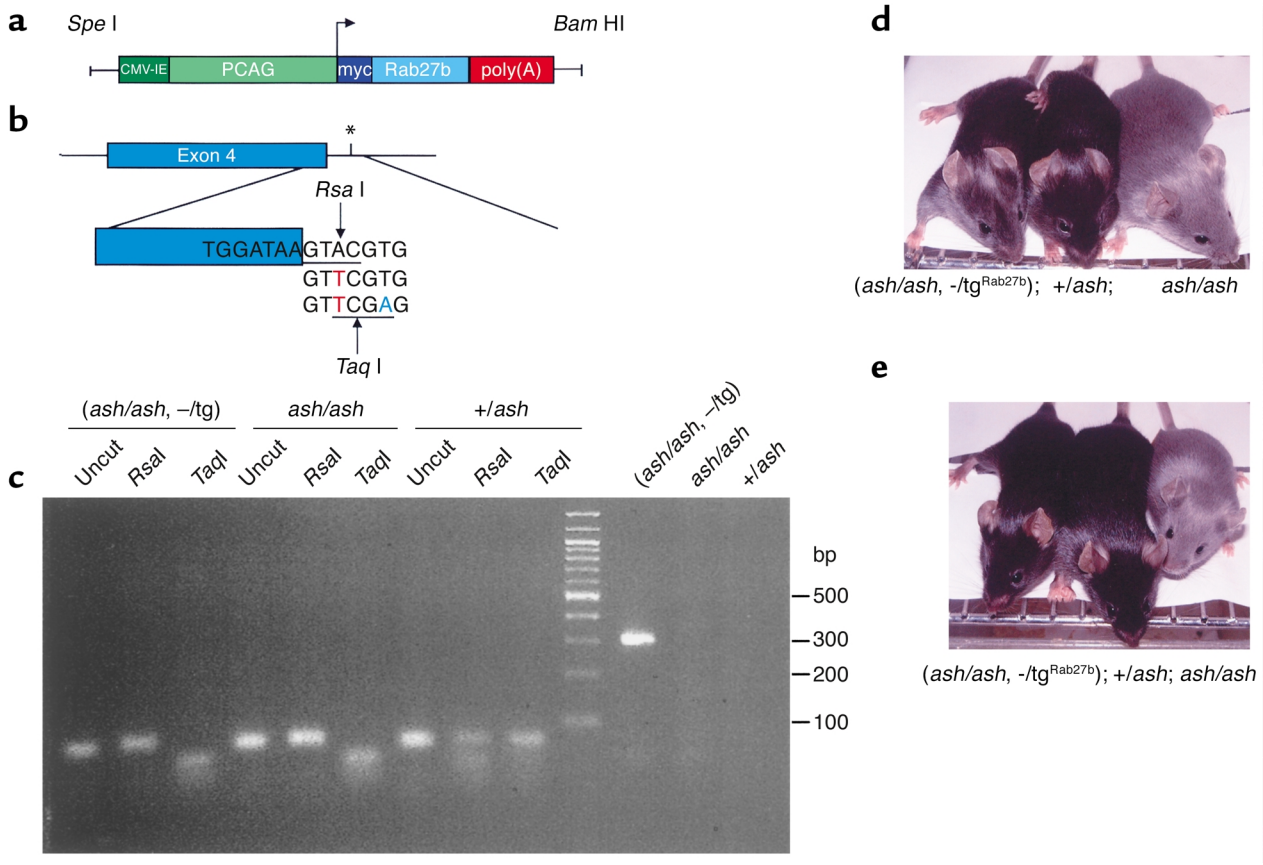

Figure 7
(**a**) Organization of the transgenic construct encoding Rab27b under the control of β-actin promoter. The P_{CAG}/mycRab27/β-globin construct contains the CMV enhancer (dark green) and the chicken β-actin promoter sequence (light green) upstream of Rab27a or Rab27b cDNA (light blue), followed by the rabbit β-globin poly(A) sequence (red). (**b**) Strategy to detect *ashen* mutation (*). This is an A→T transversion (red) that is present on the third base of the splice donor site downstream of exon 4 (blue). Primers ASH2 (see Methods), introduces a T→A transversion (green). *Rsa*I, which recognizes the sequence GTAC (underlined), cuts the DNA where indicated only in the absence of the *ashen* mutation. *Taq*I, which recognizes the sequence TCGA (underlined), cuts the DNA where indicated only if the *ashen* mutation is present. (**c**) Mouse genotyping. After PCR amplification the 80 bp product was digested with *Rsa*I and *Taq*I, which originates one fragment of 50 bp and one fragment of 30 bp. The uncut amplified product is shown as a control. The screening for the presence of the transgene was done as described in Methods, generating a product of 324 bp. The PCR and digestion products were resolved on a 3% agarose gel. The molecular weight of the standards is indicated on the right. (**d** and **e**) Photography of representative mice for Rab27b (**d**) or Rab27a (**e**) rescue experiment. Littermates resulting from crosses between a homozygous *ashen* mice with heterozygous transgenic mice were genotyped as above.

because many cells exhibited a partial phenotype and only normal cells were scored, and also because the ashen-like melanocytes grew more rapidly in culture (our unpublished observations). Furthermore, the expression levels of transgenes in melanocytes are low as suggested by immunofluorescence experiments.

Rab27a andRab27b but not other Rab's rescue ashen melanocyte phenotype. To address the specificity of Rab27 function in melanosome transport, we questioned whether other Rab proteins could induce melanosome redistribution in *ashen* melanocytes. We transiently transfected an *ashen* melanocytic cell line (melan-*ash*; ref. 18) with pEGFP-Rab1a, pEGFP-Rab3a, pEGFP-Rab27a, and pEGFP-Rab27b (Figure 9). As expected, pEGFP-Rab27a–transfected cells exhibited melanosomes distributed along dendrites without accumulation in the perinuclear region (Figure 9c). Melanocytes transfected with pEGFP-Rab27b show similar results, with the majority of cells exhibiting peripheral distribution of melanosomes along dendrites (Figure 9d). Conversely, melanocytes transfected with pEGFP-Rab1a or Rab3a showed clumping of melanosomes around the perinuclear region, as observed in nontransfected cells (Figure 9, a and b). These results suggest that Rab27a and its closely related isoform Rab27b play a specific and important role in melanosome transport.

Discussion

We present evidence that the Rab27 proteins are at least partially functionally redundant in melanocytes, suggesting that the phenotype of GS type 1 patients (and respective *ashen* mouse model) results from the relative expression of Rab27a and Rab27b in specialized cell types. In affected cell types, such as melanocytes and CTLs, Rab27b

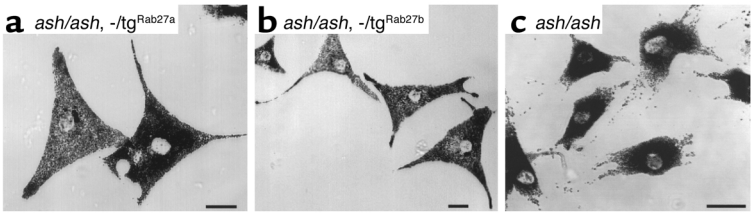

Figure 8
Melanocytes from rescued mice show normal melanosome distribution. Primary melanocytes from *ash/ash*, –/tg^{Rab27a} (**a**), *ash/ash*, –/tg^{Rab27b} (**b**), or *ash/ash* (**c**) were cultured and subjected to phase-contrast light microscopy as described in Methods. The *ash/ash* cells in **c** were derived from a littermate of *ash/ash*, –/tg^{Rab27b}. Bars, 20 μM.

expression is undetectable. However, platelets and other cell types where Rab27b is expressed remain apparently normal in GS. Transgenic expression of Rab27b in cultured melanocytes and *ashen* mice result in normal melanosome transport in melanocytes and rescue of the coat color defect. Taken together, our results suggest functional compensation of Rab27a by Rab27b in melanocytes.

We analyzed the expression patterns of Rab27a and Rab27b in mouse tissues by immunoblot analysis after producing non–cross-reacting Ab's. We report that Rab27b is more selectively expressed than Rab27a, confirming and extending previous reports using RT-PCR (31), Northern blotting (40), and immunoblotting (39). The immuno-EM studies point to a similar localization for both Rab27 isoforms. Rab27a and Rab27b decorate primarily the limiting membrane of dense granules but are also observed around α-granules. Colocalization of Rab27 isoforms suggest functional redundancy between the Rab27 proteins.

The existence of a platelet phenotype in *ashen* mice was carefully investigated for two reasons. First, platelets express both Rab27a and Rab27b and provide an opportunity to study the function of these proteins. Second, a platelet phenotype in *ashen* mice was reported recently despite no such reports from human GS patients (16). In contrast to the results presented by Wilson et al. (16), we found no evidence of bleeding tendency, SPD, or platelet-dense granule defects in *ashen* mice obtained from frozen stocks at The Jackson Laboratory and containing the reported mutation in the *Rab27a* gene (ref. 16; Figure 7). Our data are consistent with studies of GS patients. In the original description of the syndrome, platelet function was analyzed in one patient, and no defects were found (12). Subsequently, we could not find descriptions of platelet defects in reported cases. Additionally, a previous report described normal bleeding times for *ashen* mice (22). Our results clearly indicate that platelets exhibit normal function and morphology in the presence of a Rab27a loss-of-function mutation. One possible explanation is that the mouse colony used by Wilson et al. acquired one or more independent genetic mutations resulting in platelet SPD.

The fact that *gunmetal* mice present a bleeding phenotype, which was confirmed in this study, could be explained by the nature of the mutation present in these mice. We showed previously that Rab27a is one of a few Rab's affected by the reduced activity of RGGT (19, 26). We speculate that both Rab27a and Rab27b, and a few more Rab's, are partially inactivated by the *gunmetal* mutation and that the *gunmetal* phenotype results from the additive effects of the partial dysfunctions of the affected Rab's.

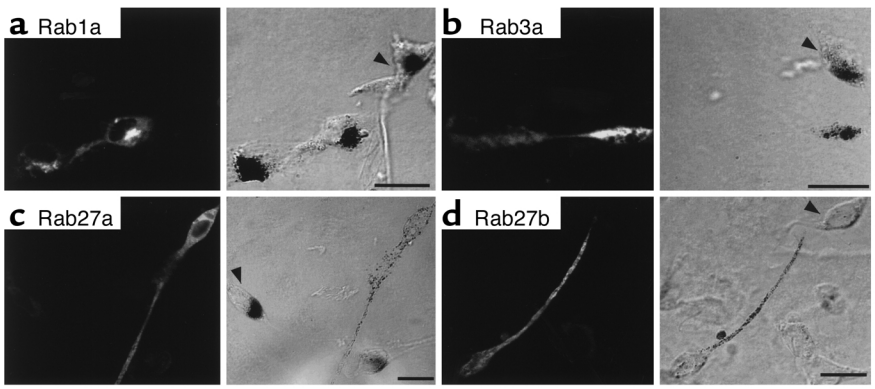

Figure 9
Transient expression of Rab proteins in *ashen* melanocytes. Melan-ash melanocytes derived from *ashen* mice were transiently transfected with pEGFP-Rab1a (**a**), pEGFP-Rab3a (**b**), pEGFP-Rab27a (**c**), and pEGFP-Rab27b (**d**) and subjected to fluorescence and phase-contrast light microscopy as described under Methods. Nontransfected cells are indicated by arrowheads. Bars, 20 μM.

In a previous study, we suggested that Rab27a and Rab27b could be functionally redundant given their related primary structure and the fact that they could both localize to melanosomes in melanocytes when overexpressed as green fluorescent protein fusions following transient transfection (31). The present data extend these previous results by demonstrating that Rab27b is able to support melanosome transport in melanocytes in the absence of Rab27a. We present evidence at both cellular and organism levels. At the cellular level, transient overexpression of Rab27a or Rab27b in *ashen* melanocytes leads to peripheral distribution of melanosomes, as observed in wild-type melanocytes. This effect is specific for the Rab27 proteins because neither Rab1a nor Rab3a overexpression resulted in peripheral melanosome movement. The inability of Rab3a to act in melanosome motility is particularly relevant because it is one of the closest homologs of Rab27 (7) and reported to be associated with melanosomes (42, 43).

In melanocytes, Rab27a appears to function in melanosome transport by recruiting melanophilin (encoded by the *leaden* gene) and myosin Va (encoded by the *dilute* gene), thereby allowing the retention of melanosomes at the cell periphery through the binding to the actin cytoskeleton (38, 44–49). We, and others, have also shown recently that Rab27b also interacts specifically with melanophilin (38, 48). The ability of Rab27b to bind Rab27a effectors appears to be the molecular basis for the functional redundancy between the Rab27 isoforms reported here.

GS patients and *ashen* mice exhibit loss of CTL killing activity (13, 19). Therefore, we examined whether Rab27b could rescue the CTL phenotype in addition to coat color dilution. Neither *ash/ash,* –/tg^{Rab27a} nor *ash/ash,* –/tg^{Rab27b} exhibited CTL killing activity (G. Bossi, D.C. Barral, M.C. Seabra, and G. Griffiths, unpublished data), suggesting that the transgene is not expressed in CTLs. We then compared the expression of the transgenic proteins in CTLs with other tissues by immunoblot, but could not detect any expression. Moreover, others have obtained similar lack of expression of transgenes driven by the chicken β-actin promoter in T lymphocytes (M. Dallman, personal communication).

A specific function for Rab27b remains elusive, although the selective high expression levels of Rab27b in platelets may indicate a specific role in platelet biology. Future studies should focus on this issue. Our study suggests that the molecular description of the function of Rab27 proteins in different cell types may lead to new insights into the biology of lysosome-related organelles and of the diseases in which they are affected.

Acknowledgments

We would like to thank Giovanna Bossi and Gillian Griffiths for performing CTL killing assays on transgenic mice, Adele Hartnell for advice on the use of the FACS, Sheila Hassock for advice on platelet assays, Clare Huxley for advice on transgenesis, Dick Swank for providing mutant mice, John A. Hammer III for providing melan-ash melanocytes, Molly Strom for making the Rab3a construct, Mimi Mules for affinity purification of Ab's, and to the other members of our labs for stimulating ideas and discussions. This work was supported by a Wellcome Trust Programme grant and a Medical Research Council component grant to M.C. Seabra, a Medical Research Council programme grant to Colin Hopkins which supported L.M. Collinson, and a British Heart Foundation grant to K.S. Authi. D.C. Barral was supported by a PhD studentship, grant PRAXIS XXI, from Fundação para a Ciência e a Tecnologia, Portugal.

1. Pereira-Leal, J.B., and Seabra, M.C. 2000. The mammalian Rab family of small GTPases: definition of family and subfamily sequence motifs suggests a mechanism for functional specificity in the Ras superfamily. *J. Mol. Biol.* **301**:1077–1087.
2. Zerial, M., and McBride, H. 2001. Rab proteins as membrane organizers. *Nature Rev. Mol. Cell Biol.* **2**:107–117.
3. Segev, N. 2001. Ypt and Rab GTPases: insight into functions through novel interactions. *Curr. Opin. Cell Biol.* **13**:500–511.
4. Pfeffer, S.R. 2001. Rab GTPases: specifying and deciphering organelle identity and function. *Trends Cell Biol.* **11**:487–491.
5. Seabra, M.C., Mules, E.H., and Hume, A.N. 2002. Rab GTPases, intracellular traffic and disease. *Trends Mol. Med.* **8**:23–30.
6. Lazar, T., Gotte, M., and Gallwitz, D. 1997. Vesicular transport: how many Ypt/Rab-GTPases make a eukaryotic cell? *Trends Biochem. Sci.* **22**:468–472.
7. Pereira-Leal, J., and Seabra, M.C. 2001. Evolution of the Rab family of small GTP-binding proteins. *J. Mol. Biol.* **313**:889–901.
8. Jedd, G., Mulholland, J., and Segev, N. 1997. Two new Ypt GTPases are required for exit from the yeast trans-Golgi compartment. *J. Cell Biol.* **137**:563–580.
9. Benli, M., Doring, F., Robinson, D.G,. Yang, X., and Gallwitz, D. 1996. Two GTPase isoforms, Ypt31p and Ypt32p, are essential for function in yeast. *EMBO J.* **15**:6460–6475.
10. Singer-Kruger, B., et al. 1994. Role of three rab5-like GTPases, Ypt51p, Ypt52p, and Ypt53 in the endocytic and vacuolar protein sorting pathways of yeast. *J. Cell Biol.* **125**:283–298.
11. Horazdovsky, B.F., Busch, G.R., and Emr, S.D. 1994. VPS21 encodes a rab5-like GTP binding protein that is required for the sorting of yeast vacuolar proteins. *EMBO J.* **15**:1297–1309.
12. Griscelli, C., et al. 1978. A syndrome associating partial albinism and immunodeficiency. *Am. J. Med.* **65**:691–702.
13. Ménasché, G., et al. 2000. Mutations in RAB27A cause Griscelli syndrome associated with haemophagocytic syndrome. *Nat. Genet.* **25**:173–176.
14. Marks, M., and Seabra, M.C. 2001. The melanosome: membrane dynamics in black and white. *Nat. Rev. Mol. Cell Biol.* **2**:738–748.
15. Bahadoran, P., et al. 2001. Rab27a: a key to melanosome transport in human melanocytes. *J. Cell Biol.* **152**:843–850.
16. Wilson, S.M., et al. 2000. A mutation in Rab27a causes the vesicle transport defects observed in *ashen* mice. *Proc. Natl. Acad. Sci. USA.* **97**:9733–7938.
17. Hume A.N., et al. 2001. Rab27a regulates the peripheral distribution of melanosomes in melanocytes. *J. Cell Biol.* **152**:795–808.
18. Wu, X., et al. 2001. Rab27a enables myosin Va-dependent melanosome capture by recruiting the myosin to the organelle. *J. Cell Sci.* **114**:1091–1100.
19. Stinchcombe, J.C., et al. 2001. Rab27a is required for regulated secretion in cytotoxic T lymphocytes. *J. Cell Biol.* **152**:825–834.
20. Haddad, E.K., Wu, X., Hammer, J.A., III, and Henkart, P.A. 2001. Defective granule exocytosis in Rab27a-deficient lymphocytes from Ashen mice. *J. Cell Biol.* **152**:835–842.
21. Huizing, M., Anikster, Y., and Gahl, W.A. 2000. Hermansky-Pudlak syndrome and related disorders of organelle formation. *Traffic.* **1**:823–835.
22. Swank, R.T., Novak, E.K., McGarry, M.P., Rusiniak, M.E., and Feng, L. 1998. Mouse models of Hermansky-Pudlak syndrome: a review. *Pigment Cell Res.* **11**:60–80.
23. Swank, R.T., et al. 1993. Inherited abnormalities in platelet organelles and platelet formation and associated altered expression of low molecular weight guanosine triphosphate-binding proteins in the mouse pigment mutant gunmetal. *Blood.* **81**:2626–2635.

24. Novak, E.K., et al. 1995. Inherited thrombocytopenia caused by reduced platelet production in mice with the gunmetal pigment gene mutation. *Blood.* **85**:1781–1789.
25. Seabra, M.C. 2000. Biochemistry of Rab geranylgeranyl transferase. In *The enzymes.* Volume XXI. F. Tamanoi and D. Sigman, editors. Academic Press. New York, New York, USA. 131–154.
26. Detter, J.C., et al. 2000. Rab geranylgeranyl transferase alpha mutation in the *gunmetal* mouse reduces Rab prenylation and platelet synthesis. *Proc. Natl. Acad. Sci. USA*. **97**:4144–4149.
27. Pereira-Leal, J., Hume, A.N., and Seabra, M.C. 2001. Prenylation of Rab GTPases: molecular mechanisms and involvement in genetic disease. *FEBS Lett*. **498**:197–200.
28. Authi, K.S., Bokkala, S., Patel, Y., Kakkar, V.V., and Munkonge, F. 1993. Ca^{2+} release from platelet intracellular stores by thapsigargin and 2,5-di-(t-butyl)-1,4-benzohydroquinone: relationship to Ca^{2+} pools and relevance in platelet activation. *Biochem. J*. **294**:119–126.
29. Drummond, A.H., and Gordon, J.L. 1974. Rapid, sensitive microassay for platelet 5HT. *Thromb. Diath. Haemorrh*. **31**:366–367.
30. Weibel, E.R. 1979. Sterological methods. In *Practical methods for biological morphometry*. Volume 1. Academic Press. London, United Kingdom.
31. Ramalho, J.S., et al. 2001. Chromosomal mapping, gene structure and characterization of the human and murine RAB27B gene. *BMC Genet.* **2**:2.
32. Evan, G.I., Lewis, G.K., Ramsay, G., and Bishop, J.M. 1985. Isolation of monoclonal antibodies specific for human c-myc proto-oncogene product. *Mol. Cell Biol.* **5**:3610–3616.
33. Fregien, N., and Davidson, N. 1986. Activating elements in the promoter region of the chicken beta actin gene. *Gene.* **48**:1–11.
34. Niwa, H., Yamamura, K., and Miyazaki, J. 1991. Efficient selection for high-expression transfectants with a novel eukaryotic vector. *Gene.* **108**:193–199.
35. Hogan, B., Beddington, R., Costantini, F., and Lacy, E. 1994. *Manipulating the mouse embryo*. Cold Spring Harbor Laboratory Press. Cold Spring Harbor, New York, USA.
36. Huxley, C. 1998. Exploring gene function: use of yeast artificial chromosome transgenesis. *Methods.* **14**:199–210.
37. Sviderskaya, E.V., Wakeling, W.F., and Bennett, D.C. 1995. A cloned, immortal line of murine melanoblasts inducible to differentiate to melanocytes. *Development.* **121**:1547–1557.
38. Strom, M., Hume, A.N., Tarafdar, A.K., Barkagianni, E., and Seabra, M.C. 2002. A family of Rab27-binding proteins: melanophilin links Rab27a and myosin Va function in melanosome transport. *J. Biol. Chem.* **277**:25423–25430. doi:10.1074/jbc.M202574200.
39. Seabra, M.C., Ho, Y.K., and Anant, J.S. 1995. Deficient geranylgeranylation of Ram/Rab27 in choroideremia. *J. Biol. Chem*. **270**:24420–24427.
40. Chen, D., Guo, J., Miki, T., Tachibana, M., and Gahl, W.A. 1997. Molecular cloning and characterization of rab27a and rab27b, novel human Rab proteins shared by melanocytes and platelets. *Biochem. Mol. Med.* **60**:27–37.
41. Bennett, D.C., Cooper, P.J., and Hart, I.R. 1987. A line of non-tumorigenic mouse melanocytes, syngeneic with the B16 melanoma and requiring a tumour promoter for growth. *Int. J. Cancer.* **39**:414–418.
42. Araki, K., et al. 2000. Small GTPase Rab3A is associated with melanosomes in melanoma cells. *Pigment Cell Res.* **13**:332–336.
43. Scott, G. and Zhao, Q. 2001. Rab3a and SNARE proteins: potential regulators of melanosome movement. *J. Invest. Dermatol.* **116**:296–304.
44. Matesic, L.E., et al. 2001. Mutations in Mlph, encoding a member of the Rab effector family, cause the melanosome transport defects observed in leaden mice. *Proc. Natl. Acad. Sci. USA.* **98**:10238–10243.
45. Provance, D.W., James, T.L., and Mercer, J.A. 2002. Melanophilin, the product of the leaden locus, is required for targeting of myosin-Va to melanosomes. *Traffic.* **3**:124–132.
46. Hume, A.N., et al. 2002. The leaden gene product is required with Rab27a to recruit myosin Va to melanosomes in melanocytes. *Traffic.* **3**:193–202.
47. Wu, X.S., et al. 2002. Identification of an organelle receptor for myosin-Va. *Nat. Cell Biol.* **4**:271–278.
48. Fukuda, M., Kuroda, T.S., and Mikoshiba, K. 2002. Slac2-a/melanophilin, the missing link between Rab27 and myosin Va. *J. Biol. Chem*. **277**:12432–12436.
49. Nagashima, K., et al. 2002. Melanophilin directly links Rab27a and myosin Va through its distinct coiled-coil regions. *FEBS Lett.* **517**:233–238.